

Waseem Siddique,¹ Aneeq Raheem,¹ Muhammad Aqeel,² Sualeh Qayyum,²
Tareq Salamen,³ Khalid Waheed,² Kamran Qureshi¹

Evaluation of thermal performance factor for solar air heaters with artificially roughened channels

Heat transfer augmentation has become the utmost industrial desire. Turbulence promoters seems to be a better option for better heat transfer but at the expense of enormous pressure drop. In the current study, experimental optimization of heat transfer and pressure drop in various configurations of ribbed and corrugated surfaces on the bottom wall of the Solar Air Heater channel, having aspect ratio of 26:5 was performed. The results were evaluated in terms of enhancement in heat transfer (Nu/Nu_s), friction factor ratio (f/f_s) and thermal performance factor (η). Three different cases and nine configurations with a pitch to rib/corrugation height ratio of 4.0 were studied. Case A consists of a smooth, continuous square rib, inline and staggered broken ribs. Case B comprises 30°, 45°, 60° and 90° trapezoidal corrugated geometries while case C is the comparison of smooth, wavy corrugated and the best configurations of cases A and B. The results show that rectangular duct with staggered broken ribs and trapezoidal corrugation at 45° are the best configurations for case A and B, respectively. The 45° corrugated configuration is the best one amongst all, with values of 1.53, 1.5 and 1.33% for Nu/Nu_s , f/f_s and η respectively.

Nomenclature

Abbreviations

CNC	Computer Numerical Control	config.	Configuration
correl.	Correlation	SAH	Solar Air Heater

✉ Waseem Siddique, e-mail: waseem@pieas.edu.pk

¹Department of Mechanical Engineering, Pakistan Institute of Engineering & Applied Sciences, Nilore, Islamabad, Pakistan.

²Department of Nuclear Engineering, Pakistan Institute of Engineering & Applied Sciences, Nilore, Islamabad, Pakistan.

³Sustainable and Renewable Energy Engineering Department, University of Sharjah, United Arab Emirates.



Symbols

A	Area (m^2)
D_h	Hydraulic diameter (m)
h	Coefficient of convective heat transfer ($\text{W}/\text{m}^2\text{K}$)
k	Thermal conductivity ($\text{W}/\text{m}\cdot\text{K}$)
l_c	Length of the roughened test-section (m)
\dot{m}	Mass flow rate (kg/sec)
R	Resistance of heating coils (Ω)
T	Temperature ($^\circ\text{C}$)
v	Velocity of air (m/s)
V	Voltage applied across heater (V)
P	Pressure (Pa)
$\Delta T/\Delta x$	Temperature gradient (K/m)
ΔT	Temperature difference ($^\circ\text{C}$ or K)
e	Rib height (m)
P	Rib/Groove pitch (m)
p	Dimension of the inclined side of trapezoidal groove (m)
q	Dimension of the upper flat side of trapezoidal groove (m)
Q_{total}	Total power supplied (W)
Q_{lost}	Power lost (W)
Q	Net power supplied (W)
Q''	Heat flux (W/m^2)
x	Dimension in x -direction (m)
y	Dimension in y -direction (m)
A_{HT}	Heat transfer area (m)
A_{HT-R}	Area of ribbed plate (m)
A_s	Area of smooth plate (m)
A_{ribs}	Area of smooth plate covered by ribs (m)
A_{HT-T}	Heat transfer area of trapezoidal grooved plate (m)
A_{HT-W}	Heat transfer area of wavy grooved plate (m)
A_f	Flow area (m)
h_c	Height of the channel (m)
w_c	Width of the channel (m)
Greek symbols	
Δ	Difference
η	Thermal performance factor
ρ	Density (kg/m^3)
θ	Angle (rad)

δ	Differential change
μ	Dynamic viscosity of air (Pa·s)
Dimensionless terms	
e/D_h	Blockage ratio
f	Coefficient of friction (Darcy friction factor)
f/f_s	Friction factor ratio
Nu	Nusselt number
Nu/Nu _s	Heat transfer enhancement
P/e	Pitch to rib height ratio
Re	Reynolds number
n	Number of thermocouples
N	Number of grooves
Subscripts	
total	Total heat
i	Insulating material
HT	Heat transfer
lost	Lost (out flux)
s	Smooth
$HT-R$	Ribbed plate
ribs	Ribbed roughened
$HT-T$	Trapezoidal grooved plate
$HT-W$	Wavy corrugated plate
ss	Steady-state
c	Channel
f	Flow
circular	Circular conduit
air	Air as cooling medium
h	Hydraulic

1. Introduction

With the increase in the world population, the demand for energy is increasing day by day. The world's economy is strongly dependent on fossil fuel, which is the non-renewable source of energy. Moreover, fossil fuels produce greenhouse emissions which are responsible for global warming, climatic changes, and environmental pollution. These issues are triggering the scientists, engineers and environmentalists to look for alternate sources of energy, which are environmental friendly and can be renewed easily. Renewable energy sources like solar, wind, hydro and geothermal are potential energy sources and they have the capacity to

mitigate environmental impacts. Solar energy has the widest scope of all the renewables because it is a clean, convenient, sustainable, safe, abundant and cheapest source of energy. Almost 3,850,000 exajoules (EJ) of energy is absorbed by the atmosphere, clouds, oceans, and land in a year which is almost two times the energy that can ever be produced by incorporating all the non-renewable energy resources [1].

Solar Air Heater (SAH) is one of the applications of solar energy, used for various purposes due to an ease in installation. It is used for desalination, space heating, drying crops, and laundry and process industry. Solar air collector is the main component of SAH which is used for the conversion of solar energy to thermal energy. A solar collector generally consists of the main absorber plate, transparent sheet on the exposed side of the absorber plate, back plate, insulation below the back plate. Air flows between the passage of the front and back plate and gets heated.

SAH has generally low efficiencies due to the low thermal capacity of air and low heat transfer coefficient between air and the absorbing plate. This leads to the need for efficient techniques to increase heat transfer in SAHs. A broad range of theoretical as well as experimental work has been performed by researchers, to enhance heat transfer by investigating the effect of various turbulators [2–5], pin fin arrays [6], dimples [7], rib tabulators [8], matrix [9] and corrugation [10] in flow channels.

Ribs are the most common method of increasing heat transfer in SAH. Xu et al. [11] performed the experimental study of heat transfer in a ribbed tube of solar heater. It was interpreted that heat transfer increase by ribbed tube is 2.24 times in case of laminar flow and 3.3–5.2 times in the case of turbulent flow as compared to the smooth tube. Moreover, a correlation for Nusselt number and friction factor was developed in terms of Reynolds number and Prandtl number. Sivakandhan et al. [12] demonstrated that an increase of 22.4% in thermal efficiency is achieved in the case of parallel pass hybrid duct SAH with inclined ribs as compared to the smooth channel. Dehariya et al. [13] performed the experimental study of discrete squared-ribbed two-pass SAH. It was determined that Nusselt number is higher for the ribbed channel because of the formation of secondary vortices, flow separation and reattachment zones. The maximum enhancement in Nusselt number appeared to be 3.96 times that of the smooth channel. At the relative roughness pitch of 10, the value of the Nusselt number was found maximum. Moreover, an empirical correlation was developed in terms of relative roughness pitch. Liou et al. [8] investigated the heat transfer characteristics using a rib-roughened channel with one surface in a fully developed flow regime. A temperature-time trace for a flow in a ribbed channel was developed. A correlation for Nusselt number based on the pitch to rib height ratio and Reynolds number was developed.

The most important parameter for heat transfer enhancement is the profile of rib. Alfarawi et al. [14] performed experiments with rectangular ribbed geometries of innovative design. The bottom of the test section was roughened using semi-

circular, rectangular and hybrid rib geometries while maintaining the rib pitch to height ratio from 6.6 to 53.5. Experiments were performed by varying the Reynolds number between 12500 and 86500. The results showed that the heat transfer was enhanced between 1.3 and 2.14 while the friction factor ratio varied between 1.8 and 4.2. Tanda et al. [15] performed experiments using square and V-shaped ribs and concluded that the ribs distribution features for the heat transfer enhancement are strongly related to the rib shape and geometry. Kesharwani et al. [16] investigated the heat transfer augmentation by using 90° artificial squared ribs. The air velocity was varied between 1 m/s to 3 m/s during the tests. Enhancement in Nusselt number was achieved ranging between 1.98 and 2.84.

The second important parameter for heat transfer enhancement is the arrangement of ribs. Kumar et al. [17] showed that the thermal-hydraulic performance of discrete staggered rib pieces was better than continuous and discrete multiple V-ribs. Jin et al. [18] compared the thermal performance of a staggered and in-line arrangement of ribs on the absorber plate of SAH. It was concluded that multiple staggered arrangements of V-shaped ribs have better performance than the corresponding in-line arrangement, with an 18% increase in thermal-hydraulic performance factor. It was also reported that, for an in-line arrangement of ribs, primary vortexes and subsidiary vortexes, produced by the inter rib spacing are the main modes of heat transfer but for the staggered case, due to gap flow, two competing effects are produced which further increases the heat transfer. Bisht et al. [19] in his study exhibited that multiple V-ribs with gaps increase the local heat transfer coefficient because it gives multiple passages for the release of air streams which energizes the stagnant boundary layer flow behind the ribs and aids in better movement of air near the heated wall. Kumar et al. [20] in his study inferred that the staggered arrangement of multiple V-ribs in SAH increases heat transfer efficiently because of the creation of the supplementary turbulence as a result of flow separations and attachments. Yadav et al. [21] proved that square-sectioned transverse rib roughened SAH, having relative roughness pitch equal to 10.71 and relative roughness height equal to 0.042 presents the best thermal-hydraulic performance factor among different configurations of square-sectioned ribbed channel. Acharya et al. [22] came up with an idea of the periodically ribbed duct. They conducted several experiments to estimate heat transfer augmentation and friction factor characteristics for two Reynolds numbers, i.e., 3400 and 24000. Square ribs were introduced at the bottom plane of the channel having a pitch to rib height ratio of 20. They found two local maxima of Nusselt number at each inter-rib segment. Chandra et al. [23] performed experiments to study the friction behavior and heat transfer in a rectangular channel for Reynolds numbers range from 10,000 to 80,000 by varying the number of ribbed walls. It was observed that heat transfer increases up to 6% using ribs over both walls as compared to the corrugation on a single wall. It was further enhanced up to 5% using ribs on the three walls as compared to the two ribbed walls. Heat transfer can be further enhanced up to 7% by adding ribs on the fourth ribbed wall.

Besides arrangement of ribs, angle of ribs was also studied in the past. Abdel-Moneim et al. [24] investigated the amplification of heat transfer and the effect of flow friction using a rectangular duct with V-shaped ribs at three different angles (i.e., 30° , 45° , 60°) at the bottom wall. Experiments were performed at Reynolds number ranging from 15000 to 75000 at a rib-to-pitch ratio between 0.0375 and 0.15. It was found that the V-shaped ribs produce a secondary flow which then interacts with the main flow stream, hence, promoting turbulence and heat transfer enhancement along with the increase in flow friction. Gupta et al. [25] observed that 60° broken ribs provided higher heat transfer efficiency than 90° continuous ribs. Siddique et al. [26] numerically analyzed the heat transfer enhancement along with pressure drop in a two-pass rectangular test section by varying the aspect ratio and introducing the ribs along the flow path at an angle of 45° . It was concluded that the secondary flow generated by the ribs interacts with the bend-induced secondary flow resulting in better heat transfer characteristics. Han et al. [27] experimentally investigated the heat transfer in nine rib configurations i.e., 60° and 45° crossed ribs, 90° rib, 60° and 45° parallel ribs, 60° and 45° V-shaped ribs, and 60° and 45° Λ -shaped ribs. It was concluded that V-shaped ribs perform better than parallel ribs, subsequently greater than crossed ribs. It was also inferred that 60° and 45° perform better than 90° ribbed channel. The V-shaped ribbed channel has the highest heat transfer while Λ -shaped channel has the maximum pressure drop losses. Smallest heat transfer and pressure drop were observed in the case of the cross arrangement of ribs.

Heat transfer augmentation through corrugated surfaces along with other innovative geometries and orientations have been an inspiring technique for investigators. Corrugation performs two functions. Firstly, it creates turbulence that results in a boundary layer separation from the wall. This separation and reattachment along with the vortex shedding due to turbulence provide the route for higher heat transfer. Secondly, it increases the surface area, which affects the heat transfer directly. Sunden et al. [28] performed experiments in various smooth tubes and corrugated channels to investigate the heat transfer augmentation and pressure drop for the Reynolds numbers range of 800 to 5000. It was concluded that the corrugated channel provides 3.5 times higher heat transfer as compared to the smooth channel while the pressure drop increases by 5–6 times. Salameh et al. studied the heat transfer enhancement ratio and thermo-hydraulic performance index for varying Reynold number range of 8000 to 20000 for the bent part of two-pass channel, roughened with square ribs of different configuration along the outer wall of bend [29–33]. Layek et al. [34] performed experiments using a rectangular channel with one of its walls having a combination of chamfered rib and grooved roughness to investigate the heat transfer phenomenon. It was inferred that the Nusselt number ratio and the friction factor coefficient ratio were increased by a factor of 3.24 and 3.78, respectively, as compared to the smooth channel. Furthermore, the chamfer angle was estimated along with an optimum value pitch for maximum augmentation of heat transfer for their channel. Elshafei et al. [35] conducted experiments

to study the effects of phase shift and the effect of the channel spacing for the Reynolds number range of $3220 < Re < 9420$ in a corrugated channel. It was found that the average heat transfer coefficient was enhanced 2.6 to 3.2 times but the pressure drop ratio increases by the factor of 1.9 to 2.6 as compared to the parallel configuration. Xia et al. [36] performed the numerical and experimental investigation of a complex corrugated microchannel. It was concluded that the thermal enhancement of 1.24 can be achieved at Reynolds number value of 611. Wan et al. [37] performed the numerical and experimental investigation of pressure drop and heat transfer in a half corrugated microchannel for the low range of Reynolds number. It was concluded that the lowest pressure drop was obtained in the case of half corrugated channel as compared to the flat channel. Moreover, the relative thermal-hydraulic performance index of half corrugated channels was higher than that of the double-corrugated microchannel. Tokgoz et al. [38] studied the heat transfer enhancement in corrugated ducts for different aspect ratios of the corrugation. It was inferred that corrugated walls have a prominent effect on heat transfer and pressure drop. About 30% increase in thermal performance factor was concluded for an aspect ratio of 0.3 and Reynolds number of 3000. Gao et al. [39] compared the thermal performance of wavy type cross corrugated and flat solar heaters for different orientations and operating conditions. It was depicted that cross corrugated channels have much superior performance as compared to the flat ones. Moreover, higher thermal performance was observed for the case of wavy absorbing plate along the flow direction and wavy bottom plate normal to the flow direction. Yassen et al. [40] studied the effect of corrugation in integral SAH for house-hold use and it was reported that the temperature rise is greater in case of corrugated absorber plate.

Geometric parameters and shape of corrugation are very important factors to increase the heat transfer. Many researchers presented a comparative study of different configurations of corrugation. Tyagi et al. [41] studied the thermal-hydraulics of different types of configurations in a flow channel. Among diamond, square, triangular and cylindrical corrugations, it was demonstrated that the triangular corrugations have the maximum efficiency. Brodnianska [42] experimentally studied the convective heat transfer for triangular, trapezoidal and wing corrugated heat transfer surfaces in the rectangular channels for different gap heights. Maximum Nusselt number was observed for the trapezoidal offset with a 40 mm gap height and highest value of Reynolds number while optimal value was observed for 50 mm gap height. Kumar et al. [10] compared the W-Shaped corrugation and smooth channel for SAHs numerically. It was depicted that the corrugation effectively increases the heat transfer with a maximum value of thermal performance factor of 1.2357 at a mass flow rate of 0.015kg/s. Khoshvaght-Aliabadi et al. [43] investigated that sinusoidal corrugation has a higher thermal performance factor than flat and trapezoidal type corrugation, while the highest Nusselt number and pressure drop were obtained for trapezoidal type corrugation. Manjunath et al. [44] performed the numerical study of the sinusoidal corrugated absorber plate. It was

concluded that due to higher turbulence, the heat transfer increases effectively, with maximum improvement in the thermal efficiency of 12.5% for aspect ratio of 1.5 and non-dimensional wave parameter of 1 as compared to the flat plate collector.

Besides the profile of corrugation, the angle of corrugation is also an important parameter which affects the heat transfer and pressure drop of channels. Olsson et al. [45] experimentally studied the effect of angled V-shaped ribs for a range of Reynolds number and aspect ratio. It was concluded that heat transfer in the case of angled ribs was far better than a straight ribbed channel. Naphon et al. [46] performed experiments to analyze the influence of geometric variations using wavy plates at opposite sides. Their experiments cover the range of $2000 < Re < 9000$ at a constant heat flux. It was concluded that the wavy plate shows better heat transfer characteristics as compared to smooth. Experiments were performed for the tilt angle of 20° , 40° and 60° over a range of Reynolds number. It was deduced that the increase of wavy angle causes higher fluid re-circulations and higher swirl flow intensity in the corrugation troughs and larger surface area, and therefore, the Nusselt number also increases with increasing wavy angle. The effect of wavelength, corrugation depth, angle of inclination on heat transfer and friction coefficient were investigated by Zimmerer et al. [47]. Pehlivan et al. [48] performed the experimental study of forced convection heat transfer for 0 , 27 , 50 and $22/60^\circ$ angled corrugation channels for a range of Reynolds number and channel height of 5 and 10 mm. It was concluded that the Nusselt number is strongly dependent on the corrugation angle and it increases with the increase in corrugation angle. Sarraf et al. [49] studied the effect of angle of corrugation on flow patterns and pressure drop in the case of plate heat exchangers. O'Brian et al. [50] conducted several experiments for a corrugation angle of 30° in a duct while keeping the Reynolds number in the range of 1500 and 25000 . It was concluded that heat transfer is enhanced by a factor of 2.5 over a parallel plate heat exchanger. An investigation by Islamoglu et al. [51] was conducted using a test setup, roughened by the similar corrugation as characterized in plate heat exchangers. The corrugations were oriented with 20° angle. The Reynolds number was varied between 12000 and 64000 . It was depicted that the Nusselt number and the friction factor both increase substantially by increasing the channel height. Hamza et al. [52] conducted experiments of V-shaped corrugated duct in laminar flow regime. It was reported that heat transfer and friction coefficient greatly depend upon the angle of tilt in V-corrugated channel. Qin et al. [53] studied the effect of geometric features of the corrugated plate, inclination angle, height and pitch of the corrugation, as well as the plate spacing, etc., on the performance of air preheater, and it was concluded that thermal performance factor and pressure drop increases by increasing the corrugation angle and optimum value of heat transfer performance was achieved at 45° angle of corrugation. Mehrabian et al. [54] studied the effect of angle of corrugation on hydrodynamics and thermal properties of corrugated channels using computational aids.

The performance of SAH can be appreciably improved by adding artificially roughness in the flow channels, which makes the surface of the absorber rougher. The more the roughness of the absorber surface, the more friction is faced by the fluid to travel over the surface [55]. Passive SAHs cannot improve the thermal performance of SAH in this scenario, this requires an active devices such as the blowing or suction fan, used in order to overcome the friction losses (pressure drop) inside the SAHs [56]. Meanwhile, the enhancement in heat transfer of SAHs is required to be compared with an increase of pressure drop in terms of thermo-hydraulic performance index or thermal performance factor. A high value of thermal performance factor means that enhancement in heat transfer process dominates the increase in pressure drop [57]. Hence, a promising augmentation is ensured.

From the preceded analysis, it is noticeable that the heat transfer augmentation using corrugated passages became the prime focus of the researchers. Based on the open literature, comparative study of roughened surfaces, with various arrangements of square cross-sectioned ribs, trapezoidal grooves oriented at different angles and wavy corrugation of specific sinusoidal wave function, at same pitch to rib/corrugation height have not been yet testified. Therefore, the present work focuses on the experimental estimation of heat transfer augmentation, friction factor and thermal performance factor of turbulent flow in a rectangular channel roughened with angled corrugation, wavy corrugation, and different alignment of ribs.

To the author's knowledge, no such experimental work has been done before and this makes the current study a novel one. This is believed that this study will enhance the understanding of the subject and add knowledge in the field of Solar Air Heaters (SAHs).

2. Methodology

2.1. Experimental setup

An experimental setup has been designed and fabricated to study the heat transfer enhancement and variation in friction factor ratio in a closed rectangular channel oriented horizontally for fixed fluid flow, having the Reynolds number of 38,500 in the turbulent regime, as shown in Fig. 1.

The test rig comprises a 550 W centrifugal air blower, a 3-way valve, a vortex flowmeter, an expander section, a honeycomb at the duct entrance, a flow channel, a test section, and a differential pressure gauge. The flow channel is a rectangular duct made of a transparent acrylic sheet with an aspect ratio of 26:5. The hydraulic diameter of the flow channel is 8.4 cm and its length is 135 cm. Inside the channel, a flow straightener (honeycomb) first eliminates the eddies in flow. Then sufficient length is provided to allow a uniform velocity profile to develop inside the channel, following which the test section appears where heat transfer from the surface to air takes place. A rectangular detachable test section plate is oriented horizontally

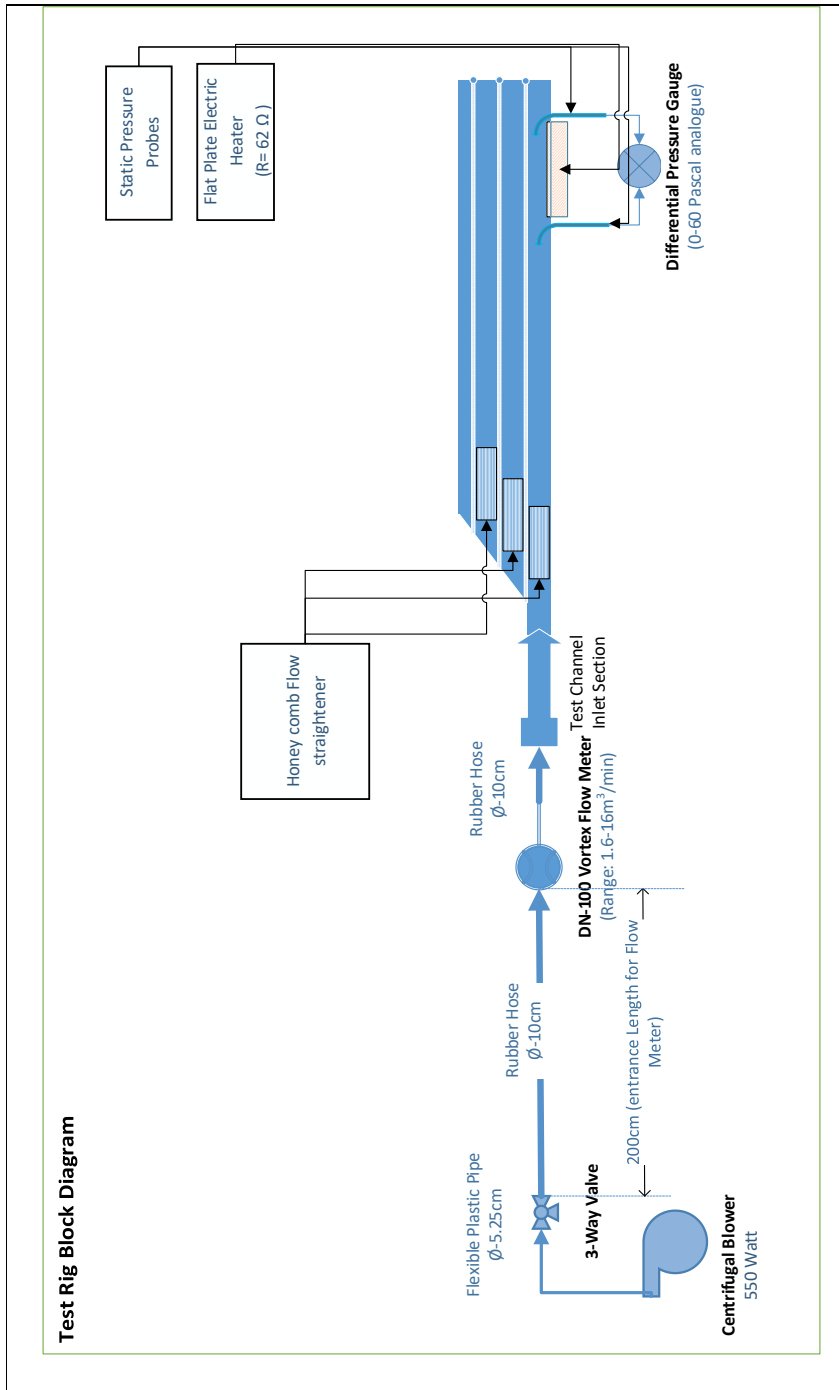


Fig. 1. Schematic of the experimental test facility

in the bottom plane of the duct. The test section plate is made up of aluminum, having 307 mm length and 5 mm thickness. The test section spans only 212 mm leaving a gap of 24 mm on either side in the channel, where airflow is unrestricted in each case and heat is not being transferred. The channel is fabricated from clear acrylics sheets (Perspex) due to good adiabatic properties as it does not conduct heat appreciably.

Instead of simulating actual solar radiations, an electric loop heater was directly attached to the channel. The heater is placed horizontally beneath the test section. The heating element of the heater is Nichrome wire having the resistance 58Ω , designed to supply a uniform heat flux of 800 W/m^2 to the absorber plate which is considered to be reasonably good value of heat energy input for testing solar air heaters [58, 59]. The heater is insulated by a reasonable thick layer of glass wool on all four sides and bottom. A variable transformer is used to adjust the voltage supplied to the heater according to the requirements. The heating power to the heater is measured by a digital multimeter with 0.58 V and 0.58Ω of accuracy. The temperature of the heated test section plate is measured using nine K-Type thermocouples, arranged in a 3×3 array as shown in Fig. 2.

One thermocouple is used to measure the ambient air temperature. The thermocouples give the reading with an uncertainty of 1.1°C . These thermocouples are connected to the USB personal data acquisition module to acquire the temperature readings. Dwyer (Magnehelic Series-2000) differential pressure gauge, with an uncertainty of 1 Pa , is used to measure the pressure drop across the test section. The flow rate of the air is measured by using the flanged type vortex flow meter (LUGB DN-100) having an operating range of $1.6\text{--}16 \text{ m}^3/\text{min}$ with an output range of $4\text{--}20 \text{ mA}$ and accuracy of 1.5% full-scale reading.

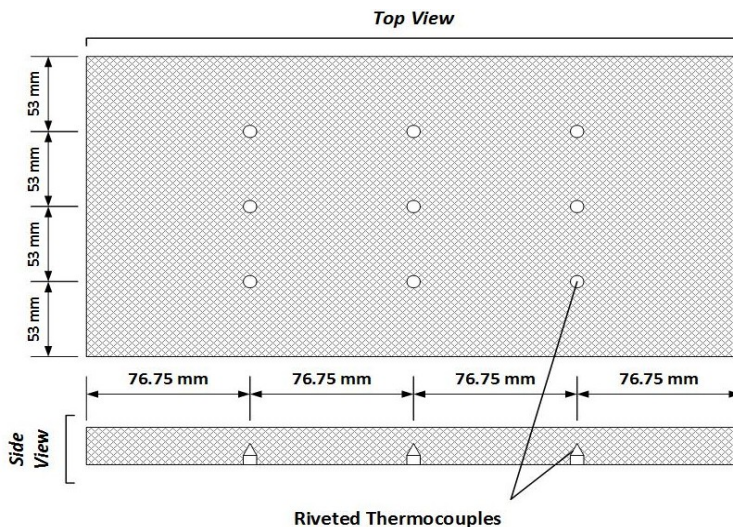


Fig. 2. Position of thermocouples in test section plate (top and side view)

2.2. Design of experiments

For the experimental setup, in the current study, the turbulent promoters are adiabatic wooden ribs of a square shape, trapezoidal and wavy corrugations grooved by CNC machine. Wood has been favored over other materials to manufacture the ribs as it is economical, readily available and has insulating properties but their turbulence effect will be the same as any other material [58]. On the other hand, aluminum was selected for the corrugated plates due to good thermal properties and easiness of machining. The different orientations of these roughness elements are categorized into nine configurations and divided into three main cases, as shown in Table 1. In all the cases, the pitch to the rib height ratio P/e parameter was kept at 4.0.

Table 1.

Test section configurations and description

Case #	Configuration #	Description
A	1	Smooth
	2	Continuous square ribbed
	3	Broken ribbed (in-line array)
	4	Broken ribbed (staggered array)
B	5	Trapezoidal 90° corrugated
	6	Trapezoidal 60° corrugated
	7	Trapezoidal 45° corrugated
	8	Trapezoidal 30° corrugated
C	1	Smooth
	9	Wavy corrugated
	–	Best configuration of case A
	–	Best configuration of case B

In the case A, a smooth aluminum plate having dimensions $307 \times 212 \times 5$ mm was used, In other configurations, the square ribs are used with a rib height value of 12.9 mm. The length of the ribs is equal to 212 mm in configuration 2 while it is equal to 42.4 mm in broken ribs configurations. The schematic diagrams of ribbed configurations of case A are shown in Fig. 3.

For the case B, the height e and pitch P of the grooves are equal to 2.5 mm and 10 mm, respectively. The pitch to the rib height ratio P/e parameter was kept at 4.0. For this case, all of these configurations are categorized based on the angle of corrugation and are shown in Fig. 4.

In the case C, sinusoidal corrugation, having the height e and pitch P of the grooves equal to 2.5 mm and 10 mm were used as shown in Fig. 5. In this case, smooth plate, sinusoidal corrugation was compared to the best configurations of case A and B.

The details of the profile of corrugation are summarized in Table 2.

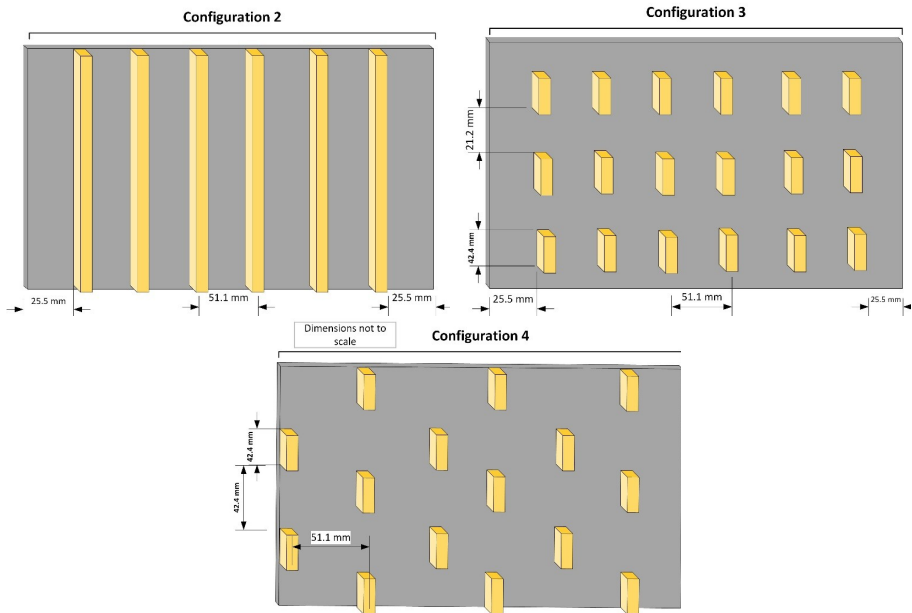
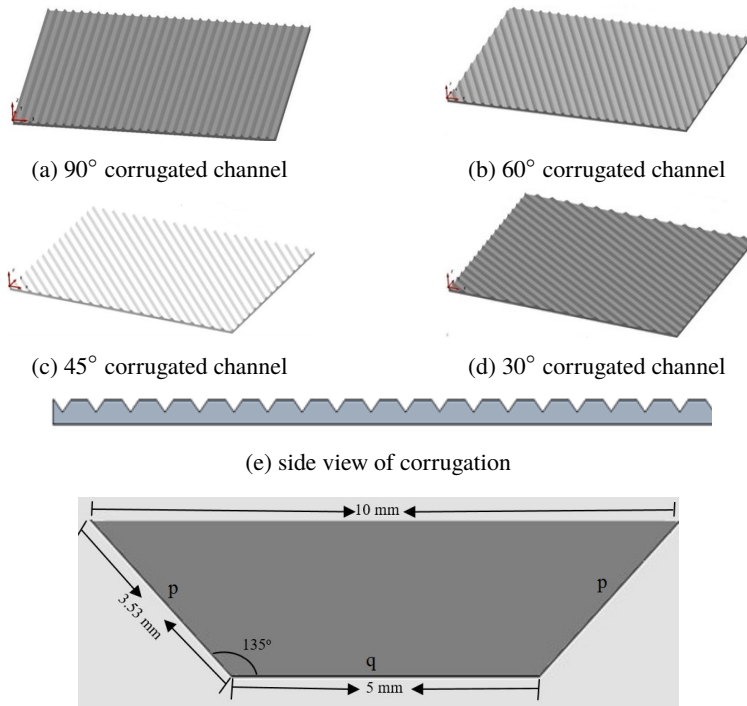


Fig. 3. Schematic diagrams of ribbed test section configurations of case A (dimension not to scale)



(f) details of trapezoidal groove (dimension not to scale)

Fig. 4. Details of test section configurations of case B

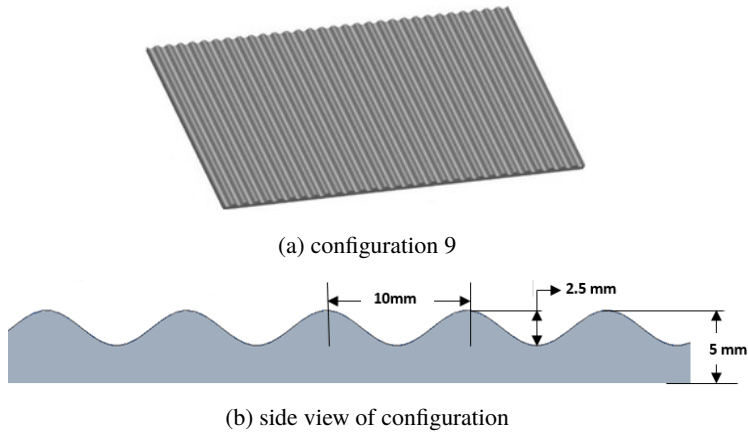
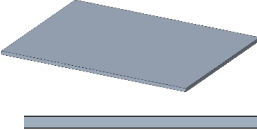

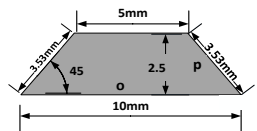
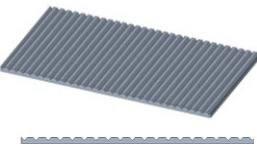
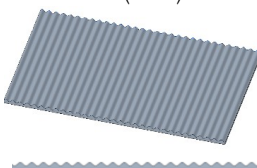


Fig. 5. Details of test section configuration 9 of case C (dimension not to scale)

Table 2.

Profiles of smooth and corrugated plates

Sr. No.	Pattern of corrugation	Profile	Flow area (mm ²)	<i>e</i> (mm)	<i>P</i> (mm)
1	Smooth (f)		$A_f = 307 \times 212$ $= 0.065 \text{ mm}^2$	–	–
2	Ribbed Config. 2 Config. 3 Config. 4		$A_{r1} = 0.049 \text{ mm}^2$ $A_{r2} = 0.056 \text{ mm}^2$ $A_{r3} = 0.0575 \text{ mm}^2$	12.9	51.5
3	Trapezoidal (t) (30°–90°)	 	$A_T = \int_a^b (o + 2p)N dy$ $= 0.785 \text{ mm}^2$ $a = 0 \text{ mm}$ $b = 212 \text{ mm}$, $N=30.7$ (number of grooves)	2.5	10
4	Sinusoidal Wavy (s)	$y = 1.25 \sin\left(\frac{2\pi}{10}x\right)$ 	$A_w = \int_a^b \int_c^d \sqrt{1 + (dy/dx)^2} dx dy$ $= 0.074 \text{ mm}^2$ $a = 0, b = 212 \text{ mm}$, $c = 0, d = 307 \text{ mm}$	2.5	10

Based upon the above configurations, a total number of 12 experiments were performed by keeping the Reynolds number at 38,500. Typically, one experiment would take about 2.5–3 hours. To remove the uncertainties, each experiment was performed thrice and a mean value was calculated.

3. Methodology of calculation

The total heat supplied per second to the test section plate can be calculated by using Eq. (1).

$$Q_{\text{total}} = \frac{V^2 \cos \theta}{R}, \quad (1)$$

where V is the voltage supplied, R is the resistance of the heating element is $\cos \theta$ the power factor and it is equal to 1 for heating elements. A fraction of the total heat input by the main heater is lost by radiation from the heating surface and conduction through the insulating material at the rear surface of the main heater. The amount of heat lost due to radiation is very small and can be ignored. Heat loss due to conduction can be evaluated by Fourier's law of conduction given by Eq. (2)

$$Q_{\text{lost}} = -k_i A_i \frac{\Delta T}{\Delta x_i}, \quad (2)$$

where i indicates the insulating material, k_i is the thermal conductivity, A_i is the cross-sectional area and $\frac{\Delta T}{\Delta x_i}$ is the thermal gradient across the insulating medium. Total heat loss estimated by Eq. (2) is approximately 10% of total heat input from the heater. The remaining heat transferred Q by forced convection to the flowing air can be calculated using Eq. (3)

$$Q = Q_{\text{total}} - Q_{\text{lost}}. \quad (3)$$

Heat flux Q'' can be estimated using Eq. (4)

$$Q'' = \frac{Q}{A_{HT}}, \quad (4)$$

where A_{HT} is the heat transfer area.

The test section plate is divided into nine test positions. For each test position, one thermocouple has been attached. Temperatures (T_{ss}) from the various nodes on the test section are recorded using the personal data acquisition device when a steady-state is achieved and mean value is calculated. The local coefficient of convective heat-transfer h is evaluated using Eq. (5)

$$h = \frac{Q''}{\Delta T_{ss}}, \quad (5)$$

where ΔT_{ss} is the temperature difference of the average temperature of the test section and ambient air temperature at a steady state. The average temperature of the test section is calculated by the arithmetic mean of temperatures of nine thermocouples of the test section.

The Nusselt number based on the hydraulic diameter D_h , thermal conductivity k and coefficient of convective heat transfer h is calculated by using Eq. (6)

$$\text{Nu} = \frac{hD_h}{k}. \quad (6)$$

Reynolds number is calculated from the air mass flow rate and hydraulic diameter by using Eq. (7)

$$\text{Re} = \frac{\dot{m}D_h}{A_f\mu}, \quad (7)$$

where \dot{m} is the mass flow rate of air, D_h is the hydraulic diameter, A_f is the flow area and μ is the dynamic viscosity of air.

The pressure drop is measured by using the differential pressure gauge. The friction factor f is estimated by the rearranged Darcy-Weisbach equation given by Eq. (8) [60]

$$f = \frac{2D_h\Delta P}{\rho l_c v^2}, \quad (8)$$

where v is the velocity of fluid. This relation has been used for the calculation of the friction factor. Blasius's correlation [61], Colebrook equation [62] and Barkic's solution [63] are based on circular conduits. The corrected friction factor for a rectangular duct can be estimated by Eq. (9) [34]

$$f = \left(1.0875 - 0.1125 \left(\frac{h_c}{w_c} \right) \right) f_{\text{circular}}, \quad (9)$$

where f_{circular} is a friction factor for circular conduits, calculated from above correlations, w_c and h_c are the width and height of the channel. This relation is used to validate the experimental friction factor with the work of Blasius's correlation [53], Colebrook equation [54] and Barkic's solution.

Enhancement in heat transfer (Nu/Nu_s) is the ratio between the Nusselt number for artificially roughened channel configuration to the Nusselt number of smooth channel configuration.

Friction factor ratio (f/f_s) is the ratio between the friction factors or pressure drops for artificially roughened channel configuration to the friction factor or pressure drop of smooth channel configuration.

The performance is measured by the Thermo-hydraulic Performance Index or Thermal Performance Factor (TPF) which is defined in Eq. (10) as the ratio between the enhancements of heat transfer to the friction factor ratio for various channels.

Greater the η value, more heat is transferred in comparison to the equivalent pressure drop across the channel.

$$\eta = \frac{(\text{Nu}/\text{Nu}_s)}{(f/f_s)^{1/3}}, \quad (10)$$

where Nu_s is the Nusselt number of a smooth channel while f_s is the friction factor of a smooth channel.

4. Results and discussion

To check the validity of the experimental setup, a comparison is made for the heat transfer results with the correlations obtained by Alfarawi et al. [14], Liou et al. [8], Sieder and Tate [64] and Gnielinski [64] and is shown in Fig. 6. The relative percentage difference of current results with the estimations of the above mentioned correlations is 15.3%, 15.2%, 15.1%, and 15.0% respectively.

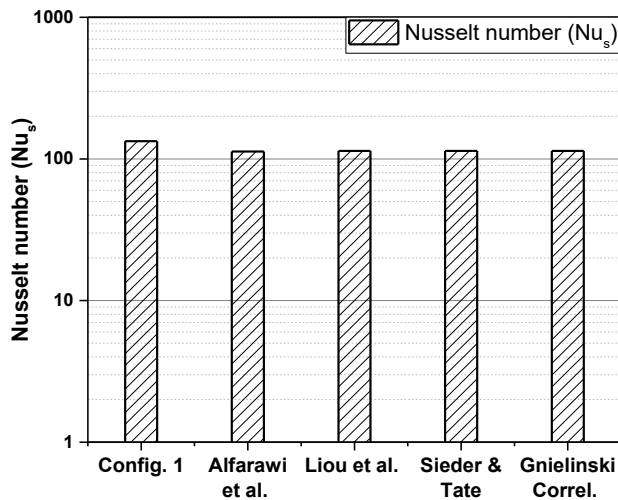


Fig. 6. Comparison of Nusselt number Nu_s of the smooth duct

Alfarawi et al. [14] and Liou et al. [8] used the rectangular duct with a hydraulic diameter D_h of 64 mm. Sieder and Tate [64] and Gnielinski [64] correlations are based on smooth circular tubes. As their geometries are slightly different compared to the current setup, therefore a small difference is understandable.

To check the results of friction factor, another comparison of the experimental results of Configuration-1 was made with the correlation of Alfarawi et al. [14], Blasius's correlation [61], Colebrook equation [62] and Barkic's solution [63] at constant Reynold number value of 38,500 and is shown in Fig. 7. The relative percentage difference of current results with the estimations of the above mentioned

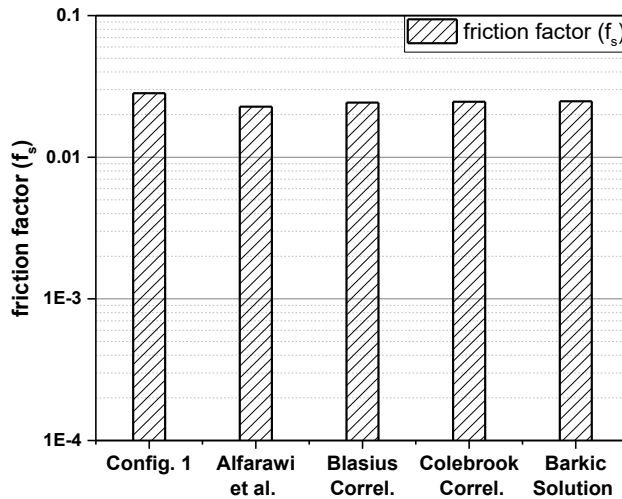


Fig. 7. Comparison of Darcy friction factor f_s of the smooth duct

researches is 19.9%, 13.9%, 13.2%, and 12.5%, respectively. These relative differences are found to be in the range of relative uncertainty of friction factor for the current test setup and a good agreement was found when comparing the present results with the correlations.

4.1. Case A

The results for normalized Nusselt numbers and friction factor ratio for case A configurations on the bottom wall of the SAH absorber channel are shown in Fig. 8. As expected, for the case of ribbed duct, higher values of Nusselt numbers are observed due to increased turbulence, but the penalty is the excessive pressure drops. Heat transfer enhancement of 1.21 times was observed for the continuous arrangement of ribs while an increase of 1.17 and 1.36 times was observed for the case of the in-line and staggered arrangement of ribs as compared to the smooth channel. This enhancement in heat transfer is equivalent to increasing in seasonal energy gain by 1.66 GJ, 1.6 GJ and 1.86 GJ for continuous, in-line and staggered arrangement of ribs, respectively [65]. The continuous ribbed arrangement has a higher friction factor ratio of 11.18 times as compared to the smooth channel, while an increase of 7.48 and 5.48 times was observed in the case of staggered and in-line arrangements.

The comprehensive results of case A configurations are given in Fig. 9. Although, Nusselt number enhanced in all ribbed configurations, but friction factor ratio increased more significantly as compared to the smooth duct. That's why the thermal performance factor is still lower than that of the smooth channel in all ribbed configurations of case A. Continuous rib configuration has the least value of thermal performance factor of 54.3 % thermal efficiency. The thermal perfor-

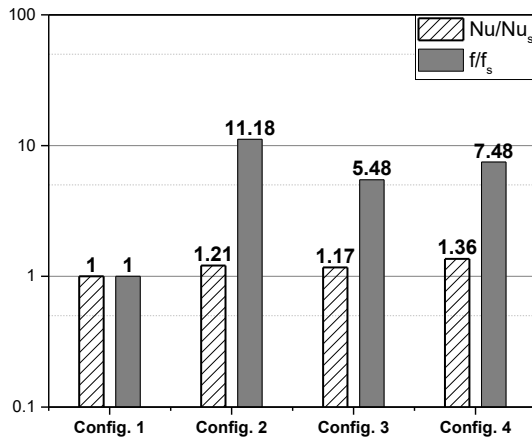


Fig. 8. Normalized Nusselt numbers Nu/Nu_s and friction factor ratio f/f_s for case A configurations

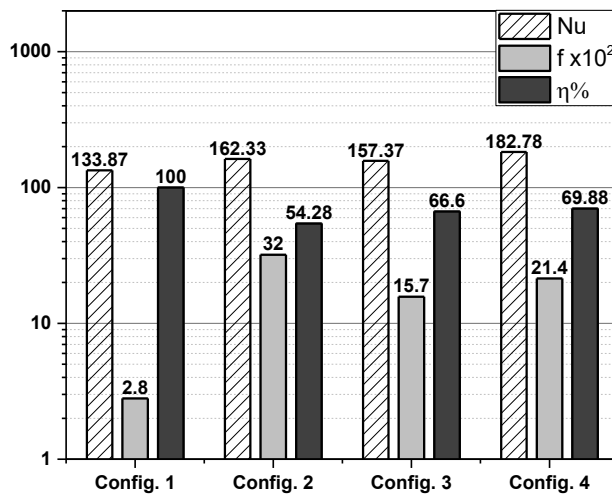


Fig. 9. Heat transfer enhancement Nu/Nu_s and friction factor ratio f/f_s results and thermal performance factor for case A configurations

mance factor of an in-line ribbed configuration is 12.3% higher than that of the continuous squared ribbed channel. Staggered broken ribs configuration is the best configuration among all configurations with thermal performance factor equal to 69.9%.

It can be inferred that broken ribs are more effective for heat transfer enhancement than continuous ribs due to stream-wise primary vortex with an inter-rib subsidiary vortex. The primary vortex improves mixing between the warmer fluid at the base of plate with the colder fluid in the mainstream, while the subsidiary vortex enhances inter-rib fluid mixing, resulting in a greater heat transfer and local heat transfer coefficient in the vicinity of the gap. The broken ribbed staggered

array configuration offers higher heat transfer enhancement than broken ribbed inline array configuration due to their arrangement. This is because, in a staggered arrangement, flow passes through the gap between the two span-wise adjacent ribs, the gap flow is distributed into three parts corresponding to their movements. The two side flows move in opposite directions and link with the neighboring inter-rib flows immediately to increase the subsidiary vortex strength. While, the central part flows through more than one gap along the stream-wise direction, undergoing reattachments, recirculations, and redevelopment of the boundary layer before uniting with the inter-rib flow further downstream. These two competing effects are responsible for further heat transfer enhancement in the staggered arrangement of ribs [18].

4.2. Case B

In the case of B, the channel with trapezoidal corrugation oriented at four different angles has been measured for the SAH absorber channel. The results for enhancement in heat transfer and friction factor ratio for case B configurations are shown in Fig. 10. The heat transfer enhancement of 1.23, 1.53, 1.57 and 1.74 was obtained for the cases of 30°, 45°, 60° and 90° grooved arrangement. This heat transfer enhancement corresponding to increasing in seasonal energy gain by 1.69 GJ, 2.1 GJ, 2.15 GJ and 2.39 GJ for the cases of 30°, 45°, 60° and 90° grooved arrangement, respectively. While friction factor ratios of 1.25, 1.5, 1.75 and 2.5 were observed in the underlying cases, the Nusselt number value increased for each configuration compared to a smooth channel. With the change in the orientation angle of corrugation, the configuration with orientation angle (90°) has the highest Nusselt number, while the configuration with orientation angle (30°) has the lowest

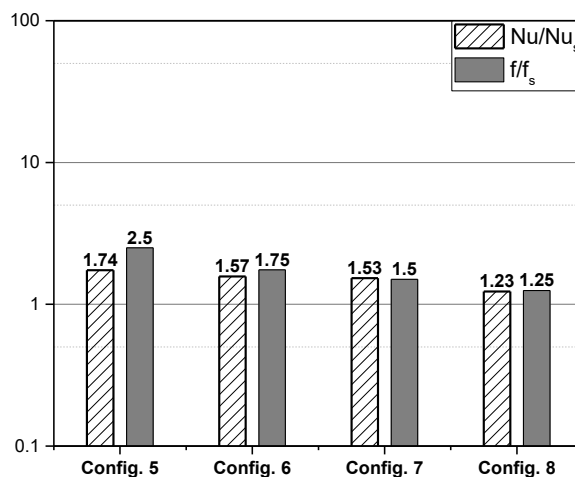


Fig. 10. Heat transfer enhancement Nu/Nu_s and friction factor ratio f/f_s for case B configurations

Nusselt number. The friction factor also increases by increasing the orientation angle for all configurations in case B.

The comparison of the thermal performance factor for case B configurations inside the SAH absorber channel is shown in Fig. 11. The thermal performance factor of 132.8%, 130.4%, 128% and 114.37% was observed for the cases of 45°, 60°, 90° and 30° grooved configuration, respectively. It is observed that the corrugation with an angle of 45° is the most efficient configuration in case B. It enhanced the heat transfer by 1.53 times while friction coefficient ratio increased by a factor of 1.5 as compared to the reference configuration. In this configuration, the thermal performance factor has enhanced up to 32.8%.

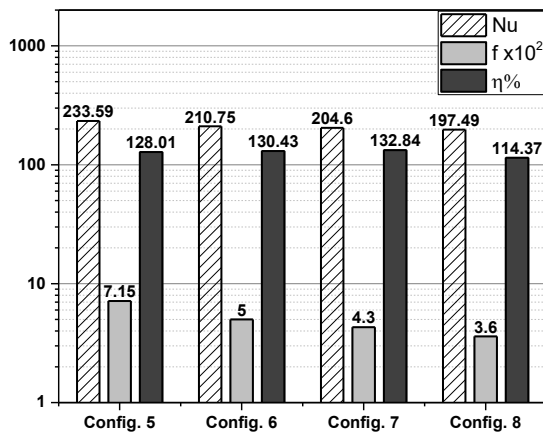


Fig. 11. Comparison of the thermal performance factor of case B configurations

So, it can be concluded that by increasing the corrugation angle, the thermal performance factor increases up to 45°, after that a decreasing trend was observed. This is because the vortices generated by the corrugation become stagnant and fluid gets struck in the troughs and form a boundary of fluid in the vicinity. As a result, fluid temperature rises near the vortices region and the coefficient of heat transfer is lowered. So, by increasing the angle of the corrugation, vortices leave the trough of grooves and subsequently join the mainstream to form a span-wise rotating secondary flow. Moreover, the swirl flow intensity of the fluid also increases in this manner. As a result, thermal performance is effectively increased by increasing the corrugation angle.

4.3. Case C

In case C, the best configuration of case A and case B, i.e., staggered broken ribbed, trapezoidal 45° corrugated and wavy corrugated configurations are compared with the smooth channel configuration of SAH absorber channel. The results for enhancement in heat transfer and friction factor ratio for case C configurations

are shown in Fig. 12. The heat transfer enhancements of 1.55, 1.53 and 1.36 were obtained for the cases of sinusoidal grooved, 45° trapezoidal grooved and broken staggered arrangement of ribs. The increasing in the seasonal energy gain was 2.13 GJ for the sinusoidal grooved ribs. While, friction factor ratios of 1.74, 1.5 and 7.48 were observed in the underlying cases. It is observed that the friction factor for trapezoidal configuration is smaller than that of wavy corrugated and broken ribbed configurations. Further, the relation in Nusselt number of case C configurations can be given as follows: the Nusselt number for the staggered broken ribbed configuration had the highest Nusselt number among all configuration, while the wavy corrugated configuration had a higher Nusselt number than the trapezoidal 45° corrugated.

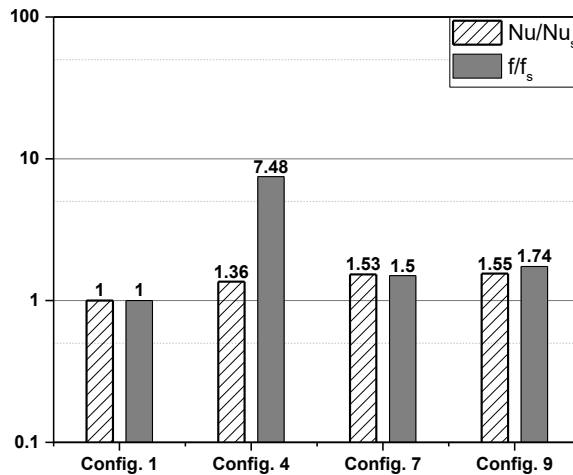


Fig. 12. Heat transfer enhancement Nu/Nu_s and friction factor ratio f/f_s result for case C configurations

The comparison of the thermal performance factor for case C configurations inside the SAHs is given in Fig. 13. The thermal performance factor of 132.8% and 128.6% were observed for the cases of 45° grooved and sinusoidal configuration. It is observed that, although sinusoidal configuration provides more heat transfer compared to other configurations, yet due to an acceptable increase in friction factor, the 45° grooved configuration gives the best results among all configuration in case of C with the thermal performance factor enhancement by 32.8% as compared to smooth channel configuration. Due to the higher enhancement heat transfer ratio in parallel to the acceptable friction factor, the overall best geometry among all the nine proposed configurations is the 45° grooved test section configuration.

So, it can be concluded that the 45° grooved is the best configuration for the thermal performance factor followed by 60° grooved and sinusoidal corrugation. The reason that can be attributed to such a trend is that in the 45° grooved configurations, fluid leaves the trough of grooves more vigorously. Instead of getting stuck

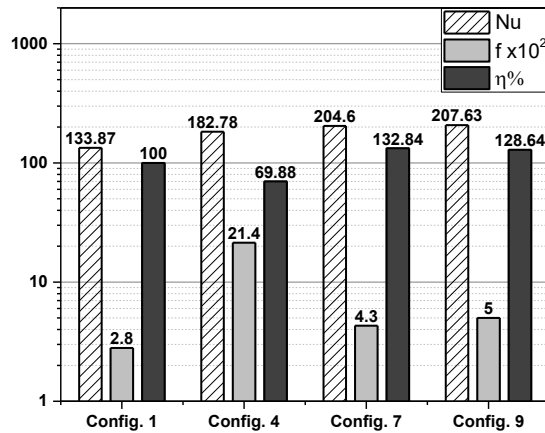


Fig. 13. Comparison of the thermal performance factor of case C configurations

in the trough region, it actively mixes with the mainstream fluid and increases secondary fluid recirculation. Due to which, heat transfer coefficient increases. Moreover, this geometry has also the reasonable value of the friction factor. So, over all thermal performance factor actively increases for the 45° grooved configuration. The uncertainties in Nusselt number, friction factor and thermal performance factor are evaluated and presented in Appendix A.

5. Conclusions

An experimental study was conducted to investigate the best geometry among ribbed and corrugated configurations for the SAH absorber channel. Three different cases of comparison have been performed.

- In case A, the rectangular channel with continuous, in-line broken and staggered broken ribs were compared to the smooth rectangular channel for SAH. Based on the thermal performance factor, a staggered broken rib configuration was found to be the best configuration. It enhances the heat transfer (Nu/Nu_s) by a factor of 1.36 while friction factor ratio (f/f_s) increases by a factor of 7.48 compared to the smooth rectangular channel. Thermal performance factor of staggered arrangement is found to be greater than continuous and inline broken arrangement of ribs.
- In the case of B, the rectangular channel was roughened with trapezoidal corrugation oriented at 90° , 60° , 45° and 30° angles for SAH. Corrugation with an angle of 45° was found the most efficient with enhancement in heat transfer by a factor of 1.53 while the ratio of the coefficient of friction increased by a factor of 1.5. In this configuration, the thermal performance factor increased by 32.8% as compared to the smooth channel.

- In case C, the best configurations of case A and case B based on the thermal performance factor and wavy corrugated configuration were compared for SAH. The increase in the friction factor was 1.5, 1.74 and 7.48 for trapezoidal corrugation oriented at 45°, wavy corrugated, and broken ribbed (staggered array) configurations, respectively, while the increase in heat transfer enhancement was 1.36, 1.53, and 1.55 for broken ribbed (staggered array), trapezoidal corrugation oriented at 45°, and wavy corrugated configurations, respectively. 45° grooved configuration gave the best results with thermal performance enhancement of 1.33 followed by sinusoidal and staggered broken ribbed configuration.
- For all the cases, 45° grooved appears to be the best configuration followed by 60° grooved, sinusoidal, 90° grooved, 30° grooved, staggered broken ribbed, inline broken ribbed and continues ribbed configurations.
- The approximately accumulative level of thermal energy gains that can be achieved throughout the season were 1.86 GJ, 2.1 GJ, and 2.13 GJ for broken ribbed (staggered array), trapezoidal corrugation oriented at 45°, and wavy corrugated configurations, respectively.
- The thermal performance factor increased by 32.85% and 28.64% for trapezoidal corrugation, oriented at 45° and wavy corrugated configurations, respectively, whereas the thermal performance factor reduced by 30.12 % for the broken ribbed (staggered array) configuration.
- Overall, the 45° grooved configuration was the best configuration amongst all configurations based on the thermal performance factor. Thanks to the applications of SAHs, with the considered configurations of air channels.

Appendix A: Error propagation calculations

Due to uncertainty in measurement in different measuring devices, the error propagates further in calculations. This propagation of errors in heat transfer coefficient, Nusselt number, friction factor and the thermal performance factor of best corrugation configuration was calculated based on the basic rules of propagation [66].

Uncertainty in Nusselt number

The mathematical relation of Nu is shown in Eq. (6). The relative error in the Nusselt number can be calculated by Eq. (A-1)

$$\frac{\delta \text{Nu}}{\text{Nu}} = \sqrt{\left[\frac{\delta h}{h}\right]^2 + \left[\frac{\delta D_h}{D_h}\right]^2}. \quad (\text{A-1})$$

To calculate the uncertainty in Nusselt number, uncertainties in heat transfer coefficient and hydraulic diameter are required.

Uncertainty in coefficient of heat transfer

The mathematical relation of the heat transfer coefficient is given in Eq. (5). The relative error in the heat transfer coefficient $\frac{\delta h}{h}$ can be calculated by Eq. (A-2)

$$\frac{\delta h}{h} = \sqrt{\left[\frac{\delta q}{q}\right]^2 + \left[\frac{\delta A}{A}\right]^2 + \left[\frac{\delta \Delta T}{\Delta T}\right]^2}. \quad (\text{A-2})$$

To calculate the relative error in the heat transfer coefficient, the relative error in heat transfer rate $\frac{\delta q}{q}$, heat transfer area $\frac{\delta A}{A}$, and temperature difference $\frac{\delta \Delta T}{\Delta T}$ are needed to calculate.

As heating power can be calculated from Eq.1, the relative error in the heat transfer rate can be calculated from Eq. (A-3)

$$\frac{\delta q}{q} = \sqrt{4 \left[\frac{\delta V}{V}\right]^2 + \left[\frac{\delta R}{R}\right]^2}. \quad (\text{A-3})$$

As the heating area can be calculated by Eq. (A-4) for smooth channel

$$A = l_c w_c, \quad (\text{A-4})$$

the relative error in the heat transfer area can be calculated by Eq. (A-5)

$$\frac{\delta A}{A} = \sqrt{\left[\frac{\delta l}{l}\right]^2 + \left[\frac{\delta w}{w}\right]^2}. \quad (\text{A-5})$$

As temperature difference can be calculated by Eq. (A-6)

$$\Delta T = T_{ss} - T_{\text{air}}, \quad (\text{A-6})$$

the relative error in temperature difference can be calculated by Eq. (A-7)

$$\frac{\delta \Delta T}{\Delta T} = \frac{1}{\Delta T} \sqrt{[\delta T_{ss}]^2 + [\delta T_{\text{air}}]^2}. \quad (\text{A-7})$$

A total of 9 thermocouples were used on the test section plate. So, uncertainty in temperature values of thermocouples can be calculated from Eq. (A-8)

$$\delta T_{ss} = \frac{\sum_{i=1}^n (T_i - T_{ss})}{n}, \quad (\text{A-8})$$

where n is the number of thermocouples.

Uncertainty in hydraulic diameter

Hydraulic diameter D_h can be calculated from Eq. (A-9)

$$D_h = \frac{4A_f}{P_w} = \frac{4h_c w_c}{2h_c + 2w_c}, \quad (\text{A-9})$$

where h_c and w_c are the height and width of the channel respectively. A_f is the flow area and P_w is the wetted perimeter. The relative error in hydraulic diameter can be calculated using Eq. (A-10)

$$\frac{\delta D_h}{D_h} = \sqrt{\left[\frac{\delta h_c}{h_c}\right]^2 + \left[\frac{\delta w_c}{w_c}\right]^2 + \frac{(\delta h_c)^2 + (\delta w_c)^2}{(h_c + w_c)^2}}. \quad (\text{A-10})$$

Uncertainty in friction factor

Darcy friction factor can be calculated from Eq. (8). The relative uncertainty in the friction factor can be calculated using Eq. (A-11)

$$\frac{\delta f}{f} = \sqrt{\left[\frac{\delta D_h}{D_h}\right]^2 + \left[\frac{\delta \Delta P}{\Delta P}\right]^2 + \left[\frac{\delta l}{l}\right]^2 + \left[2\frac{\delta v}{v}\right]^2}, \quad (\text{A-11})$$

where $\frac{\delta \Delta P}{\Delta P}$ and $\frac{\delta l}{l}$ can be calculated on the base of least count of the instrument and $\frac{\delta v}{v}$ can be calculated from Eqs. (A-12) to (A-14)

$$v = \frac{Q}{A_f}, \quad (\text{A-12})$$

$$\frac{\delta v}{v} = \sqrt{\left[\frac{\delta Q}{Q}\right]^2 + \left[\frac{\delta A_f}{A_f}\right]^2}, \quad (\text{A-13})$$

where

$$\frac{\delta A_f}{A_f} = \sqrt{\left[\frac{\delta h_c}{h_c}\right]^2 + \left[\frac{\delta w_c}{w_c}\right]^2}. \quad (\text{A-14})$$

Uncertainty in Thermal Performance Factor (TPF)

The thermal performance factor can be calculated from Eq. (10). The relative error in the thermal performance factor can be calculated by Eq. (A-15)

$$\frac{\delta \eta}{\eta} = \sqrt{\left[\frac{\delta \text{Nu}}{\text{Nu}}\right]^2 + \left[\frac{\delta \text{Nu}_s}{\text{Nu}_s}\right]^2} = \frac{1}{9} \left[\left(\frac{\delta f}{f}\right)^2 + \left(\frac{\delta f_s}{f_s}\right)^2 \right]. \quad (\text{A-15})$$

An uncertainty analysis is performed to assess the accuracy of the measurements using the basic error propagation rules. Uncertainties for Nusselt number, friction coefficient and thermal performance factor are evaluated. An uncertainty of 7.0%, 6.3%, 5.8%, 6.7%, 10.3%, 9.3%, 9.1%, 7.4% and 9.21% was observed in Nusselt number for configurations 1-9 respectively while an uncertainty of 25.2%, 3.7%, 5.4%, 4.46%, 10.4%, 14.6%, 16.97%, 20.2%, 14.59% was found in friction factor. The uncertainties in thermal performance factor for these configurations were found to be 15.46, 12.7, 12.5, 12.9, 15.42, 15.2, 15.3, 14.82, 15.1%.

Acknowledgement

The authors acknowledge the support from the Department of Nuclear Engineering and concerned authorities at PIEAS.

Manuscript received by Editorial Board, February 18, 2021;
final version, June 05, 2021.

References

- [1] W.A. Hermann. Quantifying global exergy resources. *Energy*, 31(12):1685–1702, 2006. doi: [10.1016/j.energy.2005.09.006](https://doi.org/10.1016/j.energy.2005.09.006).
- [2] T. Alam, R.P. Saini, and J.S. Saini. Use of turbulators for heat transfer augmentation in an air duct – A review. *Renewable Energy*, 62:689–715, 2014. doi: [10.1016/j.renene.2013.08.024](https://doi.org/10.1016/j.renene.2013.08.024).
- [3] A. Kumar, R.P. Saini, and J.S. Saini. Heat and fluid flow characteristics of roughened solar air heater ducts – A review. *Renewable Energy*, 47:77–94, 2012. doi: [10.1016/j.renene.2012.04.001](https://doi.org/10.1016/j.renene.2012.04.001).
- [4] D. Kumar and L. Prasad. Heat transfer augmentation of various roughness geometry used in solar air heaters. *International Journal of Mechanical Engineering and Technology*, 8(12):491–508, 2017.
- [5] R. Prakash, A.K. Singh, and P.A. Verma. The effect of roughness geometries on heat transfer enhancement in solar air heater – A review. *International Journal on Recent and Innovation Trends in Computing and Communication*, 6(4):286–291, 2018.
- [6] N.N. Sheikh, B. Kumar, and N.K. Saini. A review paper on pin fin efficiency enhancement. *International Journal of Applied Engineering Research*, 14(8):108–112, 2019.
- [7] M. Sethi, V. Goel, and N.S. Thakur. Correlations for solar air heater duct with dimpled shape roughness elements on absorber plate. *Solar Energy*, 86(9):2852–2861, 2012. doi: [10.1016/j.solener.2012.06.024](https://doi.org/10.1016/j.solener.2012.06.024).
- [8] T.-M. Liou, J.-J. Hwang, and S.-H. Chen. Simulation and measurement of enhanced turbulent heat transfer in a channel with periodic ribs on one principal wall. *International Journal of Heat and Mass Transfer*, 36(2):507–517, 1993. doi: [10.1016/0017-9310\(93\)80025-P](https://doi.org/10.1016/0017-9310(93)80025-P).
- [9] M.A. Al-Nimr. Transient behaviour of a matrix solar air heater. *Energy Conversion and Management*, 34(8):649–656, 1993. doi: [10.1016/0196-8904\(93\)90099-V](https://doi.org/10.1016/0196-8904(93)90099-V).
- [10] A. Kumar, A. Gholap, R. Gangarde, S.M. Shinde, M.P. Vyavahare, V.B. Mete, and S.A. Borude. Performance of solar air heaters with corrugated absorber plate – A CFD approach. *International Journal of Innovative Research and Advanced Studies*, 4(11):76–86, 2017.
- [11] W. Xu, S. Wang, L. Huang, Q. Wang, Q. Zhang, and H. Lu. Thermo-hydraulic performance of Therminol liquid phase heat transfer fluid in a ribbed tube of solar heater. *Renewable Energy*, 101:919–929, 2017. doi: [10.1016/j.renene.2016.09.043](https://doi.org/10.1016/j.renene.2016.09.043).

- [12] C. Sivakandhan, T.V. Arjunan, and M.M. Matheswaran. Thermohydraulic performance enhancement of a new hybrid duct solar air heater with inclined rib roughness. *Renewable Energy*, 147(1):2345–2357, 2020. doi: [10.1016/j.renene.2019.10.007](https://doi.org/10.1016/j.renene.2019.10.007).
- [13] S.K. Dehariya and A.R. Jaurker. Experimental analysis for enhancement of heat transfer in two pass solar air heater duct by using square rib in discrete geometry. *International Research Journal of Engineering and Technology*, 03(06):1839–1846, 2016.
- [14] S. Alfarawi, S.A. Abdel-Moneim, and A. Bodalal. Experimental investigations of heat transfer enhancement from rectangular duct roughened by hybrid ribs. *International Journal of Thermal Sciences*, 118:123–138, 2017. doi: [10.1016/j.ijthermalsci.2017.04.017](https://doi.org/10.1016/j.ijthermalsci.2017.04.017).
- [15] G. Tanda. Heat transfer in rectangular channels with transverse and V-shaped broken ribs. *International Journal of Heat and Mass Transfer*, 47(2):229–243, 2004. doi: [10.1016/S0017-9310\(03\)00414-9](https://doi.org/10.1016/S0017-9310(03)00414-9).
- [16] V. Kesharwani and R. Vishwakarma. Numerical investigation of heat transfer and fluid flow characteristics of square type tabulator roughness solar air heater. *International Journal of Mechanical and Industrial Technology*, 3(2):109–116, 2016.
- [17] A. Kumar and M.-H. Kim. Thermohydraulic performance of rectangular ducts with different multiple V-rib roughness shapes: A comprehensive review and comparative study. *Renewable and Sustainable Energy Reviews*, 54:635–652, 2016. doi: [10.1016/j.rser.2015.10.030](https://doi.org/10.1016/j.rser.2015.10.030).
- [18] D. Jin, J. Zuo, S. Quan, S. Xu, and H. Gao. Thermohydraulic performance of solar air heater with staggered multiple V-shaped ribs on the absorber plate. *Energy*, 127:68–77, 2017. doi: [10.1016/j.energy.2017.03.101](https://doi.org/10.1016/j.energy.2017.03.101).
- [19] V.S. Bisht, A.K. Patil, and A. Gupta. Review and performance evaluation of roughened solar air heaters. *Renewable and Sustainable Energy Reviews*, 81(1):954–977, 2018. doi: [10.1016/j.rser.2017.08.036](https://doi.org/10.1016/j.rser.2017.08.036).
- [20] A. Kumar and M.-H. Kim. Effect of roughness width ratios in discrete multi V-rib with staggered rib roughness on overall thermal performance of solar air channel. *Solar Energy*, 119:399–414, 2015. doi: [10.1016/j.solener.2015.06.030](https://doi.org/10.1016/j.solener.2015.06.030).
- [21] A.S. Yadav and J. L. Bhagoria. Modeling and simulation of turbulent flows through a solar air heater having square-sectioned transverse rib roughness on the absorber plate. *The Scientific World Journal*, 2013:ID827131, 2013. doi: [10.1155/2013/827131](https://doi.org/10.1155/2013/827131).
- [22] S. Acharya, T. Myrum, X. Qiu, and S. Sinha. Developing and periodically developed flow, temperature and heat transfer in a ribbed duct. *International Journal of Heat and Mass Transfer*, 40(2):461–479, 1997. doi: [10.1016/0017-9310\(96\)00033-6](https://doi.org/10.1016/0017-9310(96)00033-6).
- [23] P.R. Chandra, C.R. Alexander, and J. C. Han. Heat transfer and friction behaviors in rectangular channels with varying number of ribbed walls. *International Journal of Heat and Mass Transfer*, 46(3):481–495, 2003. doi: [10.1016/S0017-9310\(02\)00297-1](https://doi.org/10.1016/S0017-9310(02)00297-1).
- [24] S.A. Abdel-Moneim, E.F. Atwan, and A.R. El-Shamy. Heat transfer and flow friction in a rectangular duct with repeated multiple V-ribs mounted on the bottom wall. In *Proceedings of the 12th International Mechanical Power Engineering Conference (IMPEC12)*, pages 11–25, 2001.
- [25] A. Gupta, V. SriHarsha, S.V. Prabhu, and R.P. Vedula. Local heat transfer distribution in a square channel with 90° continuous, 90° saw tooth profiled and 60° broken ribs. *Experimental Thermal and Fluid Science*, 32(4):997–1010, 2008. doi: [10.1016/j.expthermflusci.2007.11.015](https://doi.org/10.1016/j.expthermflusci.2007.11.015).
- [26] W. Siddique, T.H. Fransson, and L.A. El-Gabry. Improved design of internally cooled trailing edge at engine similar conditions: A conjugate heat transfer problem. In *Proceedings of the ASME Turbo Expo 2012: Turbine Technical Conference and Exposition. Volume 4: Heat Transfer, Parts A and B*, pages 1357–1372. Copenhagen, Denmark. June 11–15, 2012. doi: [10.1115/GT2012-68557](https://doi.org/10.1115/GT2012-68557).

- [27] J.C. Han, Y.M. Zhang, and C.P. Lee. Augmented heat transfer in square channels with parallel, crossed, and V-shaped angled ribs. *Journal of Heat Transfer*, 113(3):590–596, 1991. doi: [10.1115/1.2910606](https://doi.org/10.1115/1.2910606).
- [28] B. Sundén and T. Sköldheden. Heat transfer and pressure drop in a new type of corrugated channels. *International Communications in Heat and Mass Transfer*, 12(5):559–566, 1985. doi: [10.1016/0735-1933\(85\)90079-X](https://doi.org/10.1016/0735-1933(85)90079-X).
- [29] T. Salameh and B. Sunden. An experimental study of heat transfer and pressure drop on the bend surface of a U-duct. In *Proceedings of the ASME Turbo Expo 2010: Power for Land, Sea, and Air. Volume 4: Heat Transfer, Parts A and B*, pages 13–21. Glasgow, UK. June 14–18, 2010. doi: [10.1115/GT2010-22139](https://doi.org/10.1115/GT2010-22139).
- [30] T. Salameh and B. Sunden. Effects of ribs on internal blade-tip cooling. In *Proceedings of the ASME 2011 Turbo Expo: Turbine Technical Conference and Exposition. Volume 5: Heat Transfer, Parts A and B*, pages 1033–1041. Vancouver, British Columbia, Canada. June 6–10, 2011. doi: [10.1115/GT2011-45118](https://doi.org/10.1115/GT2011-45118).
- [31] T. Salameh and B. Sunden. A numerical investigation of heat transfer in a smooth bend part of a U-duct. *International Journal of Numerical Methods for Heat & Fluid Flow*, 24(1):137–147, 2014. doi: [10.1108/HFF-03-2012-0066](https://doi.org/10.1108/HFF-03-2012-0066).
- [32] T. Salameh and B. Sunden. Numerical investigation of convective heat transfer and pressure drop for ribbed surfaces in the bend part of a U-duct. In *Proceedings of the ASME 2012 International Mechanical Engineering Congress and Exposition. Volume 7: Fluids and Heat Transfer, Parts A, B, C, and D*, pages 1909–1916. Houston, Texas, USA. November 9–15, 2012. doi: [10.1115/IMECE2012-85621](https://doi.org/10.1115/IMECE2012-85621).
- [33] L. Wang, T. Salameh, and B. Sunden. An experimental study of heat transfer on a smooth U-bend channel surface. In *Proceedings of the ASME 2012 International Mechanical Engineering Congress and Exposition. Volume 7: Fluids and Heat Transfer, Parts A, B, C, and D*, pages 1667–1674. Houston, Texas, USA. November 9–15, 2012. doi: [10.1115/IMECE2012-87295](https://doi.org/10.1115/IMECE2012-87295).
- [34] A. Layek, J.S. Saini, and S.C. Solanki. Heat transfer and friction characteristics for artificially roughened ducts with compound turbulators. *International Journal of Heat and Mass Transfer*, 50(23-24):4845–4854, 2007. doi: [10.1016/j.ijheatmasstransfer.2007.02.042](https://doi.org/10.1016/j.ijheatmasstransfer.2007.02.042).
- [35] E.A.M. Elshafei, M.M. Awad, E. El-Negiry, and A.G. Ali. Heat transfer and pressure drop in corrugated channels. *Energy*, 35(1):101–110, 2010. doi: [10.1016/j.energy.2009.08.031](https://doi.org/10.1016/j.energy.2009.08.031).
- [36] G. Xia, D. Ma, Y. Zhai, Y. Li, R. Liu, and M. Du. Experimental and numerical study of fluid flow and heat transfer characteristics in microchannel heat sink with complex structure. *Energy Conversion and Management*, 105:848–857, 2015. doi: [10.1016/j.enconman.2015.08.042](https://doi.org/10.1016/j.enconman.2015.08.042).
- [37] Z. Wan, Q. Lin, X. Wang, and Y. Tang. Flow characteristics and heat transfer performance of half-corrugated microchannels. *Applied Thermal Engineering*, 123:1140–1151, 2017. doi: [10.1016/j.applthermaleng.2017.05.176](https://doi.org/10.1016/j.applthermaleng.2017.05.176).
- [38] N. Tokgoz, M.M. Aksoy, and B. Sahin. Investigation of flow characteristics and heat transfer enhancement of corrugated duct geometries. *Applied Thermal Engineering*, 118:518–530, 2017. doi: [10.1016/j.applthermaleng.2017.03.013](https://doi.org/10.1016/j.applthermaleng.2017.03.013).
- [39] W. Gao, W. Lin, T. Liu, and C. Xia. Analytical and experimental studies on the thermal performance of cross-corrugated and flat-plate solar air heaters. *Applied Energy*, 84(4):425–441, 2007. doi: [10.1016/j.apenergy.2006.02.005](https://doi.org/10.1016/j.apenergy.2006.02.005).
- [40] T.A. Yassen, N.D. Mokhlif, and M.A. Eleiwi. Performance investigation of an integrated solar water heater with corrugated absorber surface for domestic use. *Renewable Energy*, 138:852–860, 2019. doi: [10.1016/j.renene.2019.01.114](https://doi.org/10.1016/j.renene.2019.01.114).
- [41] K. Tyagi. *Detailed Experimental Measurements of Heat Transfer Augmentation in Internal Channels Using a Thermochromic Liquid Crystal Technique*. Master Thesis, Virginia Polytechnic Institute and State University, Blacksburg, Virginia, USA, 2015.

- [42] Z. Brodnianska. Experimental investigation of convective heat transfer between corrugated heated surfaces of rectangular channel. *Heat Mass Transfer*, 55:3151–3164, 2019. doi: [10.1007/s00231-019-02649-3](https://doi.org/10.1007/s00231-019-02649-3).
- [43] M. Khoshvaght-Aliabadi and F. Nozan. Water cooled corrugated minichannel heat sink for electronic devices: Effect of corrugation shape. *International Communications in Heat and Mass Transfer*, 76:188–196, 2016. doi: [10.1016/j.icheatmasstransfer.2016.05.021](https://doi.org/10.1016/j.icheatmasstransfer.2016.05.021).
- [44] M.S. Manjunath, K.V. Karanth, and N.Y. Sharma. Numerical investigation on heat transfer enhancement of solar air heater using sinusoidal corrugations on absorber plate. *International Journal of Mechanical Sciences*, 138-139:219–228, 2018. doi: [10.1016/j.ijmecsci.2018.01.037](https://doi.org/10.1016/j.ijmecsci.2018.01.037).
- [45] C.-O. Olsson and B. Sunden. Thermal and hydraulic performance of a rectangular duct with multiple V-shaped ribs. *Journal of Heat Transfer*, 120(4):1072–1077, 1998. doi: [10.1115/1.2825892](https://doi.org/10.1115/1.2825892).
- [46] P. Naphon. Heat transfer characteristics and pressure drop in channel with V corrugated upper and lower plates. *Energy Conversion and Management*, 48(5):1516–1524, 2007. doi: [10.1016/j.enconman.2006.11.020](https://doi.org/10.1016/j.enconman.2006.11.020).
- [47] C. Zimmerer, P. Gschwind, G. Gaiser, and V. Kottke. Comparison of heat and mass transfer in different heat exchanger geometries with corrugated walls. *Experimental Thermal and Fluid Science*, 26(2-4):269–273, 2002. doi: [10.1016/S0894-1777\(02\)00136-X](https://doi.org/10.1016/S0894-1777(02)00136-X).
- [48] H. Pehlivan, I. Taymaz, and Y. İslamoğlu. Experimental study of forced convective heat transfer in a different arranged corrugated channel. *International Communications in Heat and Mass Transfer*, 46:106–111, 2013. doi: [10.1016/j.icheatmasstransfer.2013.05.016](https://doi.org/10.1016/j.icheatmasstransfer.2013.05.016).
- [49] K. Sarraf, S. Launay, and L. Tadrist. Complex 3D-flow analysis and corrugation angle effect in plate heat exchangers. *International Journal of Thermal Sciences*, 94:126–138, 2015. doi: [10.1016/j.ijthermalsci.2015.03.002](https://doi.org/10.1016/j.ijthermalsci.2015.03.002).
- [50] J.E. O'Brien and E. M. Sparrow. Corrugated-duct heat transfer, pressure drop, and flow visualization. *Journal of Heat Transfer*, 104(3):410–416, 1982. doi: [10.1115/1.3245108](https://doi.org/10.1115/1.3245108).
- [51] Y. Islamoglu and C. Parmaksizoglu. The effect of channel height on the enhanced heat transfer characteristics in a corrugated heat exchanger channel. *Applied Thermal Engineering*, 23(8):979–987, 2003. doi: [10.1016/S1359-4311\(03\)00029-2](https://doi.org/10.1016/S1359-4311(03)00029-2).
- [52] A.H.H. Ali and Y. Hanaoka. Experimental study on laminar flow forced-convection in a channel with upper V-corrugated plate heated by radiation. *International Journal of Heat and Mass Transfer*, 45(10):2107–2117, 2002. doi: [10.1016/S0017-9310\(01\)00309-X](https://doi.org/10.1016/S0017-9310(01)00309-X).
- [53] Y. Qin, X. Guan, Z. Dun, and H. Liu. Numerical simulation on fluid flow and heat transfer in a corrugated plate air preheater. *Journal of Chinese Society of Power Engineering*, 35:213–218, 2015.
- [54] M.A. Mehrabian and R. Poulter. Hydrodynamics and thermal characteristics of corrugated channels: computational approach. *Applied Mathematical Modelling*, 24(5):343–364, 2000. doi: [10.1016/S0307-904X\(99\)00039-6](https://doi.org/10.1016/S0307-904X(99)00039-6).
- [55] B.N. Prasad and J.S. Saini. Effect of artificial roughness on heat transfer and friction factor in a solar air heater. *Solar Energy*, 41(6): 555–560, 1988. doi: [10.1016/0038-092X\(88\)90058-8](https://doi.org/10.1016/0038-092X(88)90058-8).
- [56] S. Karsli. Performance analysis of new-design solar air collectors for drying applications. *Renewable Energy*, 32(10):1645–1660, 2007. doi: [10.1016/j.renene.2006.08.005](https://doi.org/10.1016/j.renene.2006.08.005).
- [57] H. Lu, B. Ren, Z. Pu, J. Si, F. Ren, and Y. Du. Simplified calculation of energy efficiency index for plate heat exchanger. IOP Conference Series: Earth and Environment Science, 552:12017, 2020. doi: [10.1088/1755-1315/552/1/012017](https://doi.org/10.1088/1755-1315/552/1/012017).
- [58] V.S. Hans, R P. Saini, and J.S. Saini. Heat transfer and friction factor correlations for a solar air heater duct roughened artificially with multiple V-ribs. *Solar Energy*, 84(6):898–911, 2010. doi: [10.1016/j.solener.2010.02.004](https://doi.org/10.1016/j.solener.2010.02.004).

- [59] S.K. Saini and R.P. Saini. Development of correlations for Nusselt number and friction factor for solar air heater with roughened duct having arc-shaped wire as artificial roughness. *Solar Energy*, 82(12):1118–1130, 2008. doi: [10.1016/j.solener.2008.05.010](https://doi.org/10.1016/j.solener.2008.05.010).
- [60] A. Raheem, W. Siddique, Z.H. Farooqui, T. Salameh, I. Haq, K. Waheed, and K. Qureshi. Performance evaluation of adding helical-screw tape inserts in parabolic solar trough collectors as a source of cleaner energy production. *Journal of Cleaner Production*, 297:126628, 2021. doi: [10.1016/j.jclepro.2021.126628](https://doi.org/10.1016/j.jclepro.2021.126628).
- [61] W.H. Hager. Blasius: A life in research and education. *Experiments in Fluids*, 34(5):566–571, 2003. doi: [10.1007/s00348-002-0582-9](https://doi.org/10.1007/s00348-002-0582-9).
- [62] C.F. Colebrook, T. Blench, H. Chatley, E.H. Essex, J.R. Finnicome, G. Lacey, J. Williamson, and G.G. Macdonald. Turbulent flow in pipes, with particular reference to the transition region between the smooth and rough pipe laws. *Journal of the Institution of Civil Engineers*, 11(4):133–156, 1939. doi: [10.1680/ijoti.1939.14509](https://doi.org/10.1680/ijoti.1939.14509).
- [63] D. Brkić. Solution of the implicit Colebrook equation for flow friction using Excel. *Spreadsheets in Education*, 10(2):Art.2, 2017.
- [64] T.L. Bergman, A.S. Lavine, F.P. Incropera, and D.P. DeWitt. *Fundamentals of Heat and Mass Transfer*. John Wiley & Sons, 2011.
- [65] H. Hassan, S. Abo-Elfadl, and M.F. El-Dosoky. An experimental investigation of the performance of new design of solar air heater (tubular). *Renew. Energy*, 151:1055–1066, 2020. doi: [10.1016/j.renene.2019.11.112](https://doi.org/10.1016/j.renene.2019.11.112).
- [66] R.J. Moffat. Describing the uncertainties in experimental results. *Experimental Thermal and Fluid Science*, 1(1):3–17, 1988. doi: [10.1016/0894-1777\(88\)90043-X](https://doi.org/10.1016/0894-1777(88)90043-X).